High-spin states of the semimagic nucleus ^{141}Pr

Z. Q. Li (李志泉),[1] S. Y. Wang (王守宇),[1,*] L. Liu (刘雷),[1] Y. M. Zhang (张亚梅),[1] B. Qi (亓斌),[1] S. Wang (王硕),[1] D. P. Sun (孙大鹏),[1] C. Liu (刘晨),[1] P. Zhang (张盼),[1] N. B. Zhang (张乃波),[1] H. Jia (贾慧),[1] Q. Hu (胡琪),[1] C. Y. Niu (牛晨阳),[1] Z. Q. Chen (陈志强),[1] P. Lv (吕品),[1] C. Y. Li (李传洋),[1] X. G. Wu (吴晓光),[2] G. S. Li (李广生),[2] C. Y. He (贺创业),[2] Y. Zheng (郑云),[2] C. B. Li (李聪博),[2] H. W. Li (李红伟),[2] and P. W. Luo (罗朋威)[2]

[1]*Shandong Provincial Key Laboratory of Optical Astronomy and Solar-Terrestrial Environment, Institute of Space Sciences, Shandong University, Weihai, 264209, China*

[2]*China Institute of Atomic Energy, Beijing 102413, China*

(Received 7 November 2014; revised manuscript received 27 May 2015; published 29 June 2015)

High-spin states of the semimagic nucleus ^{141}Pr have been investigated by in-beam γ-spectroscopic techniques using the fusion-evaporation ^{138}Ba(^{7}Li, $4n$) reaction at a beam energy of 38 MeV. The level scheme of ^{141}Pr has been extended up to ~6.2 MeV in excitation energy and 35/2 $\hbar$ in spin. A total of 14 new levels and 30 new transitions have been assigned to ^{141}Pr on the basis of γ-γ coincidence information. The observed level structures are discussed in light of the available experimental data and shell model calculations with the OXBASH code. According to the calculations, most of the observed levels of ^{141}Pr are from the proton excitations above the $Z = 50$ shell. Possible evidence for the neutron excitations across the $N = 82$ gap in ^{141}Pr is also discussed and compared with other $N = 82$ isotones.

DOI: 10.1103/PhysRevC.91.064319 PACS number(s): 23.20.Lv, 21.10.−k, 21.60.Cs, 27.60.+j

I. INTRODUCTION

The $N = 82$ isotones between the doubly magic nucleus ^{132}Sn and double-closed nucleus ^{146}Gd can be expected to be suitable objects for testing the shell model in the $A \sim 140$ mass region, and therefore attracted extensive experimental and theoretical interest in recent years [1–4]. From the previous experimental investigations of the excited states in these nuclei [2,5–10], it has been found that these states mostly come from various proton excitations and could be reasonably described by the shell model. In addition, for $N = 82$ isotones above ^{132}Sn, high-spin states corresponding to the neutron excitations across the $N = 82$ gap have been identified in ^{133}Sb [11], ^{134}Te, ^{135}I [12], ^{136}Xe [5], ^{137}Cs, ^{138}Ba, and also possibly in ^{139}La [2]. It would be very interesting to find out the neutron excitations across the $N = 82$ shell gap for heavier $N = 82$ isotones. To explore the systematic properties of these structure features to heavier nuclei, experiments have been performed to investigate the semimagic nucleus $^{141}_{59}$Pr$_{82}$ using the ^{138}Ba(^{7}Li, $4n$) reaction. It should be noted that, to our knowledge, it is the first time to investigate the high-spin states of ^{141}Pr using the heavy-ion fusion-evaporation reaction.

The structures of low-lying levels of ^{141}Pr have been investigated by means of β decay, transfer reactions, and inelastic scattering [13]. Prade *et al.* [14] studied the high-spin states of ^{141}Pr via ^{139}La(α, $2n$) and ^{140}Ce(d, n) reactions up to $E \sim 4.7$ MeV and spin up to 27/2 $\hbar$. In the present work, we investigate the high-spin states of ^{141}Pr using the heavy-ion fusion-evaporation reaction ^{138}Ba(^{7}Li, $4n$). The experimental procedures are described in Sec. II. The experimental results and the construction of the level scheme are presented in Sec. III. In Sec. IV, the level scheme is discussed in the light of the available experimental data and shell model calculations, and the conclusions are given in the last section.

*Corresponding author: sywang@sdu.edu.cn

II. EXPERIMENTAL DETAILS

High-spin states of ^{141}Pr were populated using the ^{138}Ba(^{7}Li, $4n$) ^{141}Pr reaction at a beam energy of 38 MeV. The beam was provided by the HI-13 tandem accelerator at the China Institute of Atomic Energy (CIAE) in Beijing. The target consisted of 3.1 mg/cm^2 of enriched (99.8%) ^{138}BaCO$_3$ rolled onto a 1.2 mg/cm^2 carbon backing. The deexcitation γ rays were detected by an array of eleven Compton-suppressed hyperpure germanium (HPGe) detectors. In addition, two planar type HPGe detectors were used to measure the x rays and low-energy γ rays. The detailed experimental setup can be found in Ref. [15]. In total, about 9×10^7 γ-γ coincidence events were recorded. In the off-line analysis, all the coincidence events were sorted into a 4096 by 4096 channel symmetrized E_γ-E_γ matrix and two asymmetric angular distribution from oriented states (ADO) [16] matrices. The multipolarities of the emitted γ rays were analyzed by means of the ADO ratio which was defined as I_γ (at ~40°)/I_γ (at ~90°). Here the γ-ray intensities (I_γ) were determined under the same gating conditions on the sum of all Ge detectors. The typical ADO ratios for stretched quadrupole or $\Delta I = 0$ dipole transitions and stretched pure dipole transitions are found to be ~1.1 and ~0.7, respectively. These values were estimated from the strong transitions of known multipolarities in ^{141}Pr [14] and ^{142}Ce [17].

III. EXPERIMENTAL RESULTS

The extended level scheme of ^{141}Pr established in the present work is shown in Fig. 1. Typical prompt γ-γ coincidence spectra for ^{141}Pr are shown in Fig. 2. The spin and parity assignments are mainly based on the measured ADO ratios of the γ rays and the previous studies [14,18]. In addition, we have extracted approximate values of the internal-conversion coefficients for the 89.7- and 91.6-keV transitions. Based on intensity balance of transitions in cascade, we have obtained

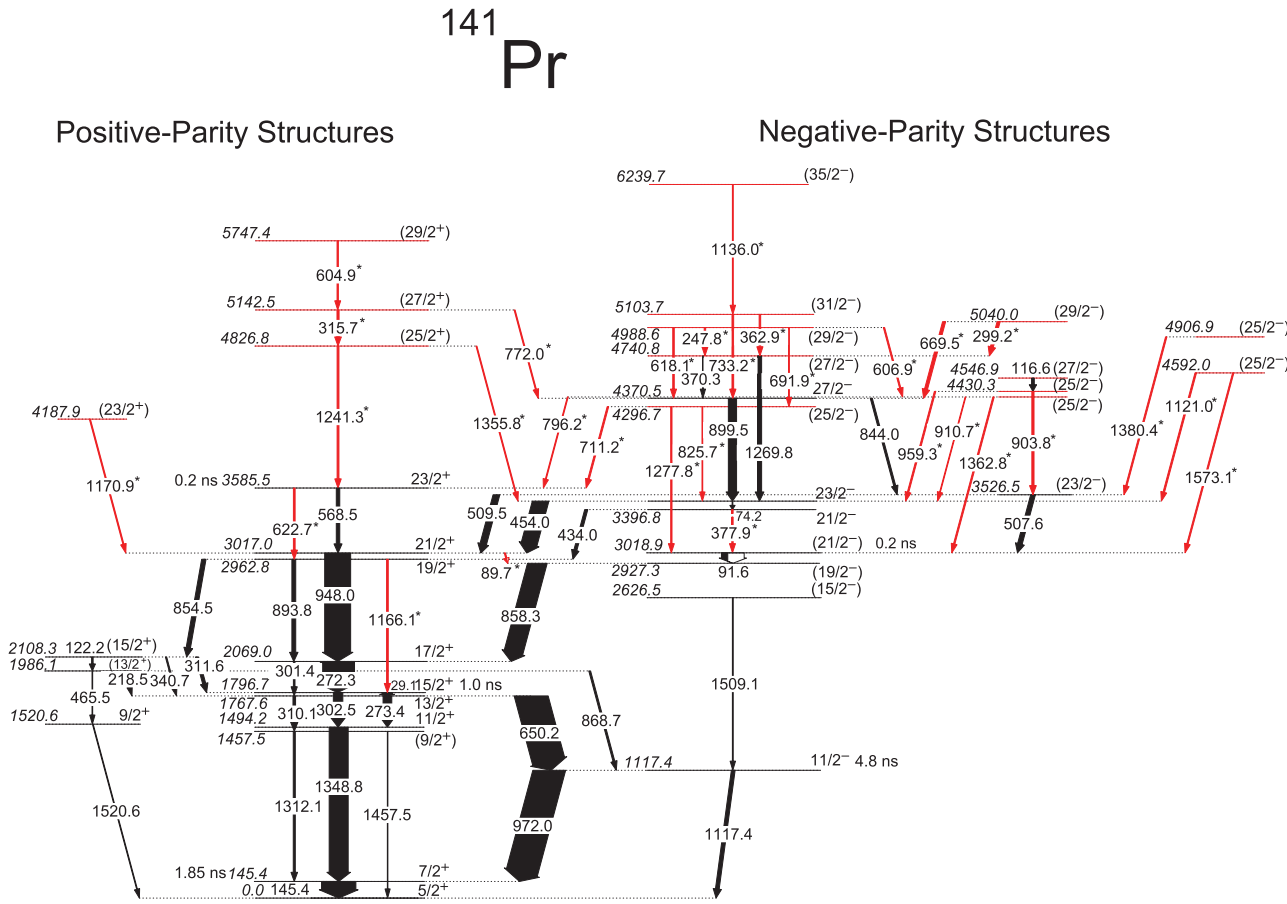

FIG. 1. (Color online) Level scheme of ^{141}Pr established in present work. New transitions and levels observed in this work are denoted in red. The newly identified transitions are also marked with asterisks.

$\alpha_{tot}(89.7) = 0.35(8)$ and $\alpha_{tot}(91.6) = 2.60(32)$, which are in good agreement with the corresponding theoretical values for $E1$ and $M1/E2$ multipolarities, respectively (see Table I). The energies and relative intensities of the observed γ rays, together with the measured ADO ratios and other relevant information concerning their placements in the level scheme are listed in Table II. The level scheme shown in Fig. 1 can be roughly separated into two parts; the left part consist of positive-parity structures and to the right are negative-parity structures. We have confirmed most of the γ rays in the previous studies [13,14,18,20]. Extensions and alterations of the level scheme with respect to previous studies are given in the following.

A. Positive-parity structures

The positive-parity yrast structures were previously observed up to $I^{\pi} = 23/2^{+}$ [14,18]. In the present work, a new cascade of γ rays with energies of 315.7, 604.9, and 1241.3 keV is identified and located above the $23/2^{+}$ level at 3585.5 keV. The ordering of the three transitions is based on the observation of two new linking transitions (772.0 and 1355.8 keV) between the positive-parity and negative-parity structures. Based on the extracted ADO ratios, the multipolarities of three transitions are found to be the $M1/E2$ character. Thus, new 4826.8-, 5142.5-, and 5747.4-keV levels are assigned as spin-parity $(25/2^{+})$, $(27/2^{+})$, and $(29/2^{+})$, respectively. Two new crossover transitions of 622.7 and 1166.1 keV are added into the positive-parity yrast sequence which feed into 2962.8- and 1796.7-keV levels, respectively. The multipolarities of the 622.7- and 1166.1-keV transitions are suggested to be $E2$ character in terms of their measured ADO ratios. In addition, the coincidence relationships suggest a level at 4187.9 keV, which decays via a new 1170.9-keV transition to the $21/2^{+}$ level at 3017.0 keV. The 1170.9-keV transition has an ADO ratio consistent with the $M1/E2$ character. Thus we assign $I^{\pi} = (23/2^{+})$ for the new 4187.9-keV level. Figure 2(a) shows a spectrum gated by the 948.0-keV transition in which most of the newly identified transitions of the positive-parity structures are observed.

B. Negative-parity structures

For the negative-parity structures, about 20 new transitions are added to the right part of Fig. 1, extending these levels to an excitation energy of ~6.2 MeV. Most of the new transitions can be clearly seen in Figs. 2(b) and 2(c). It should be noted that, based on the ADO ratio of the 711.2-keV transition (see Table II), and the observation of a 1277.8-keV crossover quadrupole transition in the present work, we change the spin value of the 3018.9-keV level from 17/2 to 21/2. In addition, the multipolarity of 91.6-keV transition have been found to be

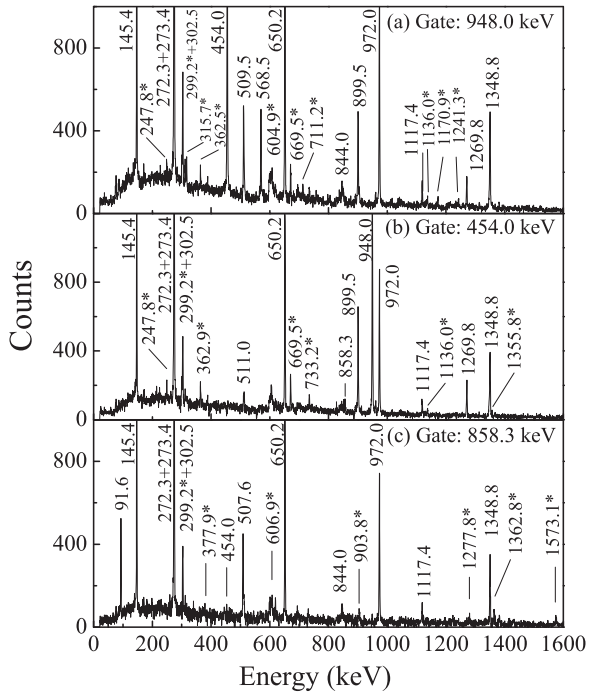

FIG. 2. Spectra of γ rays gated on the 948.0-, 454.0-, and 858.3-keV transitions, respectively. The newly observed transitions are indicated by asterisks.

$M1/E2$ based on its internal-conversion coefficient and ADO ratio, so we assign negative parity for the 3018.9-keV level. Figure 3 presents the systematics of the excitation energies for the low-lying negative-parity levels in $N = 82$ odd-A nuclei, ^{139}La [2], ^{141}Pr [14], ^{143}Pm [8,9], and ^{145}Eu [10]. As shown in Fig. 3, no $I^{\pi} = 17/2^{-}$ state above the $19/2^{-}$ level has been observed in ^{139}La or ^{143}Pm [2,8,9], instead, they all have a $21/2^{-}$ state above the $19/2^{-}$ level. The $I^{\pi} = (21/2^{-})$ assignment for the 3018.9 keV is more consistent with the systematics of $N = 82$ isotone chain. We also change the spin of 3526.5-keV level from 21/2 to 23/2 because of the present measured ADO ratio of the 507.6-keV transition showing to be dipole in character. If the 3526.5-keV level had $I^{\pi} = (21/2^{-})$, the 844.0-keV transition linking the $27/2^{-}$ level at 4370.5 keV with the 3526.5-keV level would be an $M3/E4$ transition. This would be highly unfavorable. In Ref. [14], the 116.6-keV transition was placed directly feeding the 3526.5-keV level. From the analysis of present data, we identify a new 903.8-keV transition and place it between the 4430.3- and 3526.5-keV levels. This may be corroborated by the observation of the 959.3-keV transition linking this level at 4430.3-keV into the yrast $23/2^{-}$ level at 3471.0-keV. Hence, the known 116.6-keV transition is placed above the 4430.3-keV level instead of the 3526.5-keV level.

TABLE I. Values of internal-conversion coefficients for the 89.7- and 91.6-keV transitions, the theoretical values come from the BrIcc database [19].

E_{γ}(keV)	$\alpha_{\rm tot}$(exp)	$\alpha^{th}_{\rm tot}$ ($E1$)	$\alpha^{th}_{\rm tot}$ ($M1$)	$\alpha^{th}_{\rm tot}$ ($E2$)
89.7	0.35(8)	0.338(5)	1.769(25)	3.13(5)
91.6	2.60(32)	0.319(5)	1.665(24)	2.91(4)

IV. DISCUSSION

As 50 and 82 are both magic numbers, the excited states of ^{141}Pr ($Z = 59$, $N = 82$) are expected to be mainly due to proton excitations involving three high-j orbits, $\pi g_{7/2}$, $\pi d_{5/2}$, and $\pi h_{11/2}$. The first two nearly degenerate orbits, $\pi g_{7/2}$ and $\pi d_{5/2}$, can be assumed to be filled together, thus the configurations are written as $\pi(g_{7/2}d_{5/2})^m(h_{11/2})^n$, instead of $\pi(g_{7/2})^i(d_{5/2})^j(h_{11/2})^k$, with $m + n = i + j + k = 9$. Because of the subshell closure, the low-lying states should be dominated by multiparticle (hole) excitations with $Z \leqslant 64$. The maximum value of angular momentum obtained from the $\pi(g_{7/2}d_{5/2})^9$ configuration is 23/2. The promotion of protons across subshell closure to the $\pi h_{11/2}$ orbit can provide higher angular momentum. For the positive-parity states, the complete alignment of $\pi(g_{7/2}d_{5/2})^7h^2_{11/2}$ configuration may lead to $I^{\pi} = 45/2^{+}$. The negative-parity states originate from an odd number of protons in the $\pi h_{11/2}$ orbit. The maximum value of angular momentum obtained from a $\pi(g_{7/2}d_{5/2})^8h^1_{11/2}$ configuration is 35/2.

A. Shell model calculations

In the 1960s, Wildenthal [21,22] showed that the low-spin positive-parity states of ^{141}Pr can be reasonably described in the framework of the conventional shell model using a modified surface delta interaction (MSDI). In his calculations, the nine valance protons were restricted to the $1g_{7/2}$ and $2d_{5/2}$ orbits. Additional configurations in which a single proton was excited to either the $2d_{3/2}$ or $3s_{1/2}$ orbit were also allowed. Adopting the model in Ref. [22], the high-spin states including the negative-parity states in ^{141}Pr were calculated and compared with the experimental results [14,18]. For the negative-parity states, a single proton in the $h_{11/2}$ orbit was included in the model space. So far, no calculations for ^{141}Pr have been performed in the full $Z = 50$–82 model space without truncation.

In the present work, the level structures of ^{141}Pr have been extended up to ~6.2 MeV excitation energy and 35/2 $\hbar$ spin. To get a deeper insight into the configurations of the states in ^{141}Pr, we have performed the shell model calculation using the OXBASH code [23] with the n82k interaction [24]. In this calculation, the nucleus ^{132}Sn($Z = 50$, $N = 82$) is regarded as an inert core and the remaining nine valance protons outside $Z = 50$ are distributed over the $1g_{7/2}$, $2d_{5/2}$, $2d_{3/2}$, $3s_{1/2}$, and $1h_{11/2}$ orbits without any truncation.

The calculated energies are compared with the experimental results for positive- and negative-parity states in Fig. 4. The calculated energies have been normalized with the $I^{\pi} = 5/2^{+}$ ground state of ^{141}Pr. The three strongest components (where available) of the wave functions of each state are given in Tables III and IV for positive- and negative-parity states, respectively. As shown in Fig. 4, the excitation energies and ordering of the positive-parity yrast states are very well reproduced in the present calculations. Except for the $23/2^{+}_{2}$

TABLE II. γ-ray energies, relative intensities, measured ADO ratios, initial and final level energies, and spin-parity assignments of the transitions in ^{141}Pr.

E_γ (keV)	I_γ	R_{ADO}	$E_i \rightarrow E_f$ (keV)	$I_i^\pi \rightarrow I_f^\pi$
74.2	<3		3471.0 → 3396.8	$23/2^+ \rightarrow 21/2^-$
89.7	<3		3017.0 → 2927.3	$(21/2^+) \rightarrow (19/2^-)$
91.6	18.4(2.4)	0.38(0.13)	3018.9 → 2927.3	$(21/2^-) \rightarrow (19/2^-)$
116.6	7.9(1.4)	0.95(0.38)	4546.9 → 4430.3	$(27/2^-) \rightarrow (25/2^-)$
122.2	4.4(0.9)	0.66(0.19)	2108.3 → 1986.1	$(15/2^+) \rightarrow (13/2^+)$
145.4	100.0(9.4)	1.02(0.11)	145.4 → 0.0	$7/2^+ \rightarrow 5/2^+$
218.5	2.3(0.5)		1986.1 → 1767.6	$(13/2^+) \rightarrow 13/2^+$
247.8	3.8(0.7)		4988.6 → 4740.8	$(29/2^-) \rightarrow (27/2^-)$
272.3	99.4(16.9)	0.85(0.03)	2069.0 → 1796.7	$17/2^+ \rightarrow 15/2^+$
273.4	25.4(16.9)	0.64(0.03)	1767.6 → 1494.2	$13/2^+ \rightarrow 11/2^+$
299.2	8.6(1.4)	0.74(0.18)	5040.0 → 4740.8	$(29/2^-) \rightarrow (27/2^-)$
301.4	4.4(5.7)		2069.0 → 1767.6	$17/2^+ \rightarrow 13/2^+$
302.5	27.6(5.7)	1.30(0.10)	1796.7 → 1494.2	$15/2^+ \rightarrow 11/2^+$
310.1	7.2(1.1)	1.03(0.11)	1767.6 → 1457.5	$13/2^- \rightarrow (9/2^+)$
311.6	8.6(1.3)	1.09(0.15)	2108.3 → 1796.7	$(15/2^+) \rightarrow 15/2^+$
315.7	5.7(0.9)	0.64(0.12)	5142.5 → 4826.8	$(27/2^+) \rightarrow (25/2^+)$
340.7	3.5(0.6)		2108.3 → 1767.6	$(15/2^+) \rightarrow 13/2^+$
362.9	4.3(0.6)	1.19(0.18)	5103.7 → 4740.8	$(31/2^-) \rightarrow (27/2^-)$
370.3	<2		4740.8 → 4370.5	$(27/2^-) \rightarrow 27/2^-$
377.9	<2		3396.8 → 3018.9	$21/2^- \rightarrow (21/2^-)$
434.0	8.7(1.1)	0.76(0.12)	3396.8 → 2962.8	$21/2^- \rightarrow 19/2^+$
454.0	46.5(5.2)	0.70(0.03)	3471.0 → 3017.0	$23/2^- \rightarrow 21/2^+$
465.5	<2		1986.1 → 1520.6	$(13/2^+) \rightarrow 9/2^+$
507.6	10.9(2.7)	0.76(0.08)	3526.5 → 3018.9	$(23/2^-) \rightarrow 21/2^-$
509.5	16.1(2.7)	0.60(0.05)	3526.5 → 3017.0	$(23/2^-) \rightarrow 21/2^+$
568.5	16.6(1.8)	0.65(0.07)	3585.5 → 3017.0	$23/2^+ \rightarrow 21/2^+$
604.9	3.8(0.5)	0.30(0.07)	5747.4 → 5142.5	$(29/2^+) \rightarrow (27/2^+)$
606.9	3.6(0.5)		4988.6 → 4381.7	$(29/2^-) \rightarrow (25/2^-)$
618.1	4.3(0.6)	0.54(0.13)	4988.6 → 4370.5	$(29/2^-) \rightarrow 27/2^-$
622.7	4.9(0.6)	1.10(0.25)	3585.5 → 2962.8	$23/2^+ \rightarrow 19/2^+$
650.2	95.7(9.8)	0.69(0.04)	1767.6 → 1117.4	$13/2^+ \rightarrow 11/2^-$
669.5	8.6(1.0)	0.77(0.10)	5040.0 → 4370.5	$(29/2^-) \rightarrow 27/2^-$
691.9	2.6(0.4)		4988.6 → 4296.7	$(29/2^-) \rightarrow (29/2^-)$
711.2	4.2(0.5)	0.69(0.10)	4296.7 → 3585.5	$(25/2^-) \rightarrow 23/2^+$
733.2	4.8(0.6)	1.22(0.25)	5103.7 → 4370.5	$(31/2^-) \rightarrow 27/2^-$
772.0	2.9(0.5)		5142.5 → 4370.5	$(27/2^+) \rightarrow 27/2^-$
796.2	2.5(0.5)		4381.7 → 3585.5	$(25/2^-) \rightarrow 23/2^+$
825.7	2.1(0.4)		4296.7 → 3471.0	$(25/2^-) \rightarrow 23/2^-$
844.0	5.8(0.7)	1.07(0.18)	4370.5 → 3526.5	$27/2^- \rightarrow (23/2^-)$
854.5	10.2(1.2)	1.06(0.17)	2962.8 → 2108.3	$19/2^+ \rightarrow (15/2^+)$
858.3	55.4(6.1)	0.74(0.04)	2927.3 → 2069.0	$(19/2^-) \rightarrow 17/2^+$
868.7	5.2(0.9)	0.71(0.10)	1986.1 → 1117.4	$(13/2^+) \rightarrow 11/2^-$
893.8	11.1(1.3)	0.40(0.05)	2962.8 → 2069.0	$19/2^+ \rightarrow 17/2^+$
899.5	23.9(2.8)	1.15(0.09)	4370.5 → 3471.0	$27/2^- \rightarrow 23/2^-$
903.8	6.2(0.8)	0.84(0.17)	4430.3 → 3526.5	$(25/2^-) \rightarrow (23/2^-)$
910.7	2.1(0.4)		4381.7 → 3471.0	$(25/2^-) \rightarrow (23/2^-)$
948.0	75.5(8.6)	1.15(0.06)	3017.0 → 2069.0	$21/2^+ \rightarrow 17/2^+$
959.3	3.6(0.5)	0.65(0.12)	4430.3 → 3471.0	$(25/2^-) \rightarrow 23/2^-$
972.0	92.4(10.6)	1.00(0.36)	1117.4 → 145.4	$11/2^- \rightarrow 7/2^+$
1117.4	10.8(1.5)	1.14(0.10)	1117.4 → 0.0	$11/2^- \rightarrow 5/2^+$
1121.0	4.2(0.6)		4592.0 → 3471.5	$25/2^- \rightarrow 23/2^+$
1136.0	2.5(0.4)		6249.7 → 5103.7	$(35/2^-) \rightarrow (31/2^-)$
1166.1	4.8(0.7)	1.31(0.26)	2962.8 → 1796.7	$19/2^+ \rightarrow 15/2^+$
1170.9	5.2(0.9)	0.66(0.12)	4187.9 → 3017.0	$(23/2^+) \rightarrow 21/2^+$
1241.3	5.3(0.8)	0.68(0.10)	4826.8 → 3585.5	$(25/2^+) \rightarrow 23/2^+$
1269.8	12.0(1.7)	1.13(0.14)	4740.8 → 3471.0	$(27/2^-) \rightarrow 23/2^-$
1277.8	3.7(0.6)	1.13(0.24)	4296.7 → 3018.9	$(25/2^-) \rightarrow 21/2^-$

TABLE II. (*Continued.*)

E_γ (keV)	I_γ	R_{ADO}	$E_i \rightarrow E_f$ (keV)	$I_i^\pi \rightarrow I_f^\pi$
1312.1	5.9(0.9)	0.69(0.12)	1457.5 → 145.4	$(9/2^+) \rightarrow 7/2^+$
1348.8	55.3(7.8)	0.89(0.07)	1494.2 → 145.4	$11/2^+ \rightarrow 7/2^+$
1355.8	2.7(0.5)		4826.8 → 3471.0	$(25/2^+) \rightarrow 23/2^-$
1362.8	3.9(0.7)	1.17(0.21)	4381.7 → 3018.9	$(25/2^-) \rightarrow (21/2^-)$
1380.4	3.8(0.6)	0.99(0.19)	4906.9 → 3526.5	$(25/2^- \rightarrow (23/2^-)$
1457.5	<2		1457.5 → 0.0	$(9/2^+) \rightarrow 5/2^+$
1509.1	2.4(0.6)		2626.5 → 1117.4	$(15/2^-) \rightarrow 11/2^-$
1520.6	2.2(0.4)		1520.6 → 0.0	$9/2^+ \rightarrow 5/2^+$
1573.1	3.6(0.7)	1.12(0.32)	4592.0 → 3018.9	$(25/2^-) \rightarrow (21/2^-)$

state, most of the nonyrast states are also well reproduced. The $23/2_2^+$ level at 4187.9 keV is about 500 keV lower than the present calculations if it is assumed to come from pure proton excitations. This discrepancy will be discussed in Sec. IV B. As shown in Table III, up to $23/2^+$ state, the observed states mainly come from the $\pi(g_{7/2}d_{5/2})^9$ configuration. The configurations of the newly observed states above the $23/2^+$ state can be well described as $\pi(g_{7/2}d_{5/2})^7 h_{11/2}^2$. From $23/2^+$ to $25/2^+$, the change of dominant configuration is that two protons are excited to the $h_{11/2}$ orbit from the $g_{7/2}$ and $d_{5/2}$ orbits. It is also clearly seen from Table III that the protons prefer to fill the $h_{11/2}$ orbit rather than the $d_{3/2}$ and $s_{1/2}$ orbits in high-spin regions.

For the negative-parity states shown in the right-hand side of Fig. 4, the calculated excitation energies are in reasonable agreement with the experimental levels. For the lowest negative-parity level $I^\pi = 11/2^-$, the difference between experimental and calculated energies is only ∼17 keV. For the yrast states, from $15/2^-$ to $29/2^-$, the calculated energies are roughly 70–340 keV lower than the observed levels. For the $31/2^-$ and $35/2^-$ states, the calculations reproduce the excitation energies about 150 keV higher than the observed levels. For the second and third excited states, the differences between calculations and experiment are within 220 keV. As we can see from Table IV, all the levels of the negative-parity states identified in the present work are dominated by the $\pi(g_{7/2}d_{5/2})^8 h_{11/2}^1$ configuration. In addition, the calculated wave functions have a significant admixture of configurations involving excitations of the $g_{7/2}$ and $d_{5/2}$ orbits. Compared to low spins, relatively less configuration mixing is observed at high spins. In short, the overall agreement of the experiment with the present shell model calculations in ^{141}Pr indicates that the full unrestricted (50–82) model space for the calculations is important.

B. Neutron excitations across the $N = 82$ gap

As mentioned in the introduction, the neutron excitations across the $N = 82$ gap have been identified in ^{133}Sb [11], ^{134}Te, ^{135}I [12], ^{136}Xe [5], ^{137}Cs, ^{138}Ba, and also possibly in ^{139}La [2]. The states generated by the neutron excitations are also expected in the $N = 82$ isotone ^{141}Pr. In the present work, a newly identified $23/2_2^+$ level at 4187.9 keV is about 500 keV lower than the corresponding state in the calculations if it

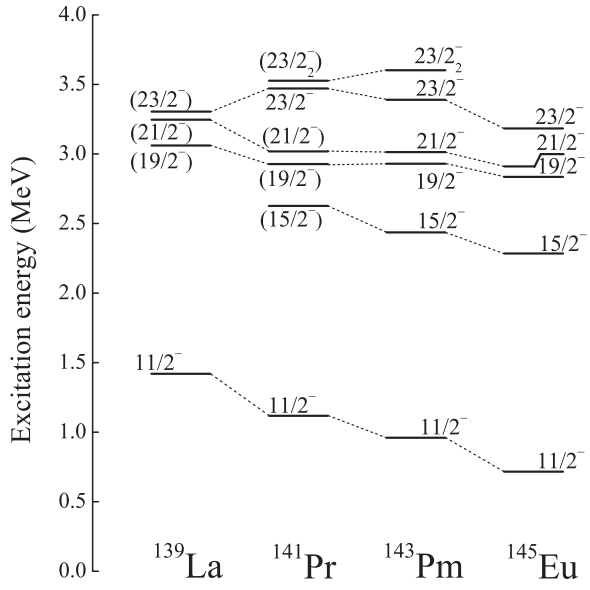

FIG. 3. The systematics of low-lying negative-parity states in the $N = 82$ odd-Z nuclei [2,8–10,14].

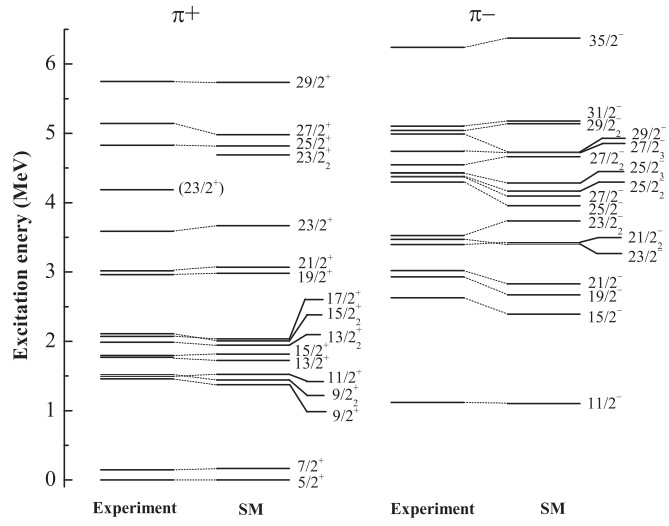

FIG. 4. Comparison of positive- and negative-parity level structures of ^{141}Pr, as proposed in the present work, with the corresponding calculated results using the OXBASH code.

TABLE III. The three strongest components of the wave functions and their partitions for positive-parity states in ^{141}Pr.

J^π	protons per orbit					Partitions
($\hbar$)	$g_{7/2}$	$d_{5/2}$	$d_{3/2}$	$s_{1/2}$	$h_{11/2}$	%
$5/2^+$	6	3	0	0	0	38.79
	8	1	0	0	0	16.89
	4	5	0	0	0	9.01
$7/2^+$	7	2	0	0	0	29.29
	5	4	0	0	0	27.82
	5	2	0	0	2	11.08
$9/2^+$	6	3	0	0	0	52.87
	5	3	1	0	0	8.46
	4	3	0	0	2	5.18
$11/2^+$	7	2	0	0	0	42.25
	5	4	0	0	0	27.74
	5	2	0	0	2	7.38
$9/2_2^+$	7	2	0	0	0	26.19
	5	4	0	0	0	24.82
	6	3	0	0	0	8.21
$13/2^+$	7	2	0	0	0	46.55
	5	4	0	0	0	21.47
	5	2	0	0	2	6.51
$15/2^+$	7	2	0	0	0	45.57
	5	4	0	0	0	26.01
	5	2	0	0	2	7.01
$13/2_2^+$	6	3	0	0	0	56.96
	4	5	0	0	0	9.74
	6	1	0	0	2	5.41
$17/2^+$	6	3	0	0	0	59.41
	4	5	0	0	0	12.90
	4	3	0	0	2	6.31
$15/2_2^+$	6	3	0	0	0	47.35
	5	4	0	0	0	14.47
	4	5	0	0	0	5.19
$19/2^+$	6	3	0	0	0	70.06
	5	4	0	0	0	12.17
	5	3	1	0	0	4.23
$21/2^+$	6	3	0	0	0	83.43
	5	4	0	0	0	4.28
	5	3	1	0	0	3.70
$23/2^+$	5	4	0	0	0	86.09
	5	2	0	0	2	5.20
	3	4	0	0	2	1.61
$23/2_2^+$	5	2	0	0	2	37.69
	7	0	0	0	2	34.11
	3	4	0	0	2	5.34
$25/2^+$	5	2	0	0	2	37.21
	7	0	0	0	2	34.87
	3	4	0	0	2	5.64
$27/2^+$	5	2	0	0	2	43.06
	7	0	0	0	2	28.21
	3	4	0	0	2	7.83
$29/2^+$	6	1	0	0	2	71.14
	4	3	0	0	2	11.17
	5	2	0	0	0	5.17

TABLE IV. The three strongest components (where available) of the wave functions and their partitions for negative-parity states in ^{141}Pr.

J^π	protons per orbit					Partitions
($\hbar$)	$g_{7/2}$	$d_{5/2}$	$d_{3/2}$	$s_{1/2}$	$h_{11/2}$	%
$11/2^-$	6	2	0	0	1	38.94
	4	4	0	0	1	16.50
	8	0	0	0	1	13.16
$15/2^-$	6	2	0	0	1	48.75
	4	4	0	0	1	12.21
	5	2	1	0	1	9.89
$19/2^-$	7	1	0	0	1	44.39
	5	3	0	0	1	29.29
	6	2	0	0	1	3.91
$21/2^-$	7	1	0	0	1	39.89
	5	3	0	0	1	34.44
	5	1	0	0	3	4.18
$23/2^-$	6	2	0	0	1	40.14
	4	4	0	0	1	15.29
	5	3	0	0	1	13.19
$21/2_2^-$	6	2	0	0	1	58.44
	4	4	0	0	1	16.30
	4	2	0	0	3	3.46
$23/2_2^-$	5	3	0	0	1	29.64
	6	2	0	0	1	21.34
	7	1	0	0	1	19.66
$25/2^-$	6	2	0	0	1	73.14
	5	3	0	0	1	8.08
	4	4	0	0	1	5.24
$27/2^-$	6	2	0	0	1	78.59
	5	3	0	0	1	4.97
	4	4	0	0	1	4.80
$25/2_2^-$	6	2	0	0	1	45.00
	5	3	0	0	1	33.19
	5	2	1	0	1	3.59
$25/2_3^-$	5	3	0	0	1	44.58
	6	2	0	0	1	29.70
	4	4	0	0	1	4.73
$27/2_2^-$	5	3	0	0	1	41.10
	4	4	0	0	1	20.31
	6	2	0	0	1	16.68
$27/2_3^-$	5	3	0	0	1	39.69
	6	2	0	0	1	36.41
	4	4	0	0	1	6.38
$29/2^-$	5	3	0	0	1	79.38
	4	2	0	0	1	3.71
	5	2	0	0	1	3.02
$29/2_2^-$	6	2	0	0	1	64.26
	4	4	0	0	1	11.02
	5	3	0	0	1	9.43
$31/2^-$	6	2	0	0	1	55.03
	4	4	0	0	1	19.27
	5	3	0	0	1	12.21
$35/2^-$	5	3	0	0	1	84.41
	4	4	0	0	1	10.97

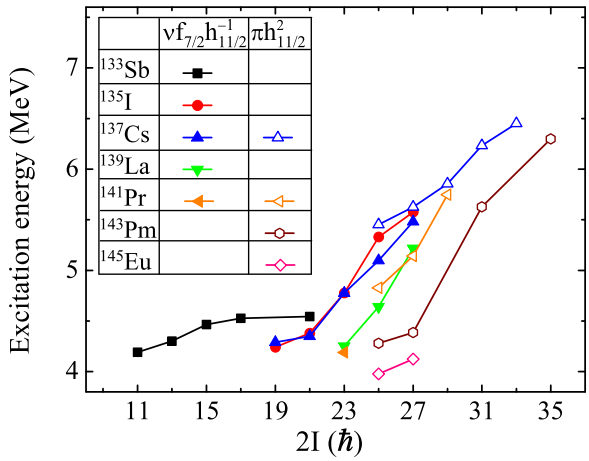

FIG. 5. (Color online) Excitation energies as a function of angular momentum of the states in the $N = 82$ odd-Z nuclei [2,8–12] proposed to be due to neutron excitations across the $N = 82$ gap and two protons excited to the $h_{11/2}$ orbit. The states generated by the neutron excitations $[\pi(g_{7/2}d_{5/2})^{(Z-50)}\nu f_{7/2}h^{-1}_{11/2}]$ and two protons excited to the $h_{11/2}$ orbit $[\pi(g_{7/2}d_{5/2})^{(Z-52)}h^{2}_{11/2}]$ are shown by the filled and open symbols, respectively.

is assumed to come from pure proton excitations. Therefore, the $23/2^+_2$ level at 4187.9 keV may come from the neutron excitations across the $N = 82$ gap and its configuration could be assigned as $\pi(g_{7/2}d_{5/2})^9\nu f_{7/2}h^{-1}_{11/2}$. Excitation energies as a function of angular momentum of the states in the $N = 82$ odd-Z nuclei [2,8–12] proposed to be due to the neutron excitations across the $N = 82$ gap and two protons excited to the $\pi h_{11/2}$ orbit are shown in Fig. 5. The states generated by the neutron excitations $[\pi(g_{7/2}d_{5/2})^{(Z-50)}\nu f_{7/2}h^{-1}_{11/2}]$ and two protons excited to the $h_{11/2}$ orbit $[\pi(g_{7/2}d_{5/2})^{(Z-52)}h^{2}_{11/2}]$ are shown by the filled and open symbols, respectively. As shown in Fig. 5, the neutron excitations across the $N = 82$ gap in ^{133}Sb [11], ^{135}I [12], ^{137}Cs, and ^{139}La [2] occur in the 4–6 MeV energy range. Their configurations are $\pi g_{7/2}\nu f_{7/2}h^{-1}_{11/2}$, $\pi g^3_{7/2}\nu f_{7/2}h^{-1}_{11/2}$, $\pi(g_{7/2}d_{5/2})^5\nu f_{7/2}h^{-1}_{11/2}$, and $\pi(g_{7/2}d_{5/2})^7\nu f_{7/2}h^{-1}_{11/2}$, respectively. The newly identified $23/2^+_2$ level at 4187.9 keV fits well into the systematics of the $N = 82$ odd-Z nuclei, thereby supporting the $\pi(g_{7/2}d_{5/2})^9\nu f_{7/2}h^{-1}_{11/2}$ configuration assignment. It is worth noting that the excitation energies of the $\pi(g_{7/2}d_{5/2})^{(Z-52)}h^2_{11/2}$ configuration decrease as the proton number increases from 55 to 63. The reason is that the proton Fermi surface becomes higher with the increasing proton number. Thereby protons are more easily excited to the $h_{11/2}$ orbit from the $g_{7/2}$ and $d_{5/2}$ orbits. Meanwhile, the energies of the states originating from the neutron excitations across the $N = 82$ gap also have a decreasing trend as the proton number increases, for example the $23/2^+$ states. As shown in Fig. 5, for the nuclei with $Z < 59$, the $\pi(g_{7/2}d_{5/2})^{(Z-50)}\nu f_{7/2}h^{-1}_{11/2}$ configuration is favorable to form the excited states. Whereas in the nuclei with $Z > 59$, the excited states are dominated by the $\pi(g_{7/2}d_{5/2})^{(Z-52)}h^2_{11/2}$ configuration. Hence, the nuclei around $Z = 59$ should have a strong competition between the $\pi(g_{7/2}d_{5/2})^{(Z-52)}h^2_{11/2}$ and $\pi(g_{7/2}d_{5/2})^{(Z-50)}\nu f_{7/2}h^{-1}_{11/2}$ configurations. This competition leads to a large mixing of these two excitation modes in ^{141}Pr. Therefore, a new effective interaction is needed to be constructed to enlarge the model space to include the neutron excitations across the $N = 82$ gap in further theoretical developments. These calculations will be expected to improve the description of the high-spin states of ^{141}Pr.

V. SUMMARY

The semimagic nucleus ^{141}Pr has been investigated using the ^{138}Ba(^{7}Li, $4n$) reaction at a beam energy of 38 MeV. The existing level scheme has been extended up to 6239.7-keV excitation energy and spin-parity value of $35/2^-$. A comparison of the experimental results with the shell-model calculations shows that the level structures of ^{141}Pr are mainly due to proton excitations above the $Z = 50$ shell. In addition, a newly identified $23/2^+_2$ level at 4187.9 keV is suggested to come from neutron excitations across the $N = 82$ gap. Further calculations, involving neutron excitations, are required to improve the understanding of the high-spin states of ^{141}Pr.

ACKNOWLEDGMENTS

We would like to thank Prof. John Sharpey-Schafer and Dr. Siyabonga Majola for a careful reading of this paper and for useful modifications. This work is supported by the National Natural Science Foundation (Grants No. 11175108 and No. 11005069), and the Independent Innovation Foundation of Shandong University IIFSDU (No. 2013ZRYQ001 and No. 2011ZRYQ004).

[1] L. Coraggio, A. Covello, A. Gargano, N. Itaco, and T. T. S. Kuo, Phys. Rev. C **80**, 044320 (2009).
[2] A. Astier *et al.*, Phys. Rev. C **85**, 064316 (2012).
[3] P. C. Srivastava, M. J. Ermamatov, and Irving. O. Morales, J. Phys. G **40**, 035106 (2013).
[4] J. K. Hwang, J. H. Hamilton, and A. V. Ramayya, Eur. Phys. J. A **49**, 125 (2013).
[5] P. J. Daly *et al.*, Phys. Rev. C **59**, 3066 (1999).
[6] R. Broda *et al.*, Phys. Rev. C **59**, 3071 (1999).
[7] James. L. DuBard, Raymond. K. Sheline, and James. B. Ball, Phys. Rev. C **3**, 1391 (1971).
[8] Sarmishtha Bhattacharya, Somen Chanda, Dipa Bandyopadhyay, Swapan. Kumar. Basu, G. Mukherjee, S. Muralithar, R. P. Singh, R. K. Bhowmik, and S. S. Ghugre, Phys. Rev. C **62**, 024317 (2000).
[9] J. J. He *et al.*, Eur. Phys J. A **9**, 157 (2000).
[10] M. Piiparinen, I. Kaunisto, R. Julin, S. Juutinen, A. Lampinen, E. Mäkelä, A. Savelius, S. Törmänen, and J. Blomqvist, Z. Phys. A **356**, 111 (1996).
[11] W. Urban, A. Zlomaniec, G. S. Simpson, H. Faust, T. Rząca-Urban, and M. Jentschel, Phys. Rev. C **79**, 037304 (2009).
[12] C. T. Zhang *et al.*, Phys. Rev. Lett. **77**, 3743 (1996).

[13] J. K. Tuli, Nucl. Data Sheets **23**, 529 (1978).
[14] H. Prade, W. Enghardt, H. U. Jäger, L. Käubler, H.-J. Keller, and F. Stary, Nucl. Phys. A **370**, 47 (1981).
[15] S. Y. Wang *et al.*, Phys. Rev. C **86**, 064302 (2012).
[16] M. Piiparinen *et al.*, Nucl. Phys. A **605**, 191 (1996).
[17] Ts. Venkova *et al.*, Eur. Phys. J. A **34**, 349 (2007).
[18] W. Enghardt, H. Prade, H. U. Jäger, L. Käubler, H.-J. Keller, F. Stary, and L. K. Kostov, Ann. Phys. (Leipzig) **498**, 424 (1986).
[19] ENSDF database, http://www.nndc.bnl.gov/ensdf/.
[20] M. Kortelahti, M. Piiparinen, A. Pakkanen, T. Komppa, and R. Komu, Phys. Scr. **24**, 10 (1981).
[21] B. H. Wildenthal, Phys. Rev. Lett. **22**, 1118 (1969).
[22] B. H. Wildenthal, Phys. Lett. B **29**, 274 (1969).
[23] B. A. Brown *et al.*, OXBASH for Windows, MSU-NSCL Report No. 1289 (2004).
[24] H. Kruse and B. H. Wildenthal, Bull. Am. Phys. Soc. **27**, 725 (1982).